PAPER B

A NUMERICAL SOLUTION FOR THE SCALAR SCATTERING EQUATION USING A MOMENT METHOD WITH BILINEAR BASIS FUNCTIONS

Jerry M. Harris and Feng Yin

ABSTRACT

We present a new moment method of solving the acoustical scattering equation. We describe the formulation, the implementation, and numerical testing of the method. The main characteristic of this method is that a bilinear basis function is used instead of a pulse basis function to evaluate the Green function, total field, and scattering potential at any arbitrary point of the image region. In this way, the integral equation may be discretized to arbitrary fineness in order to increase the accuracy of the computations. From simulation tests, we find that this method is accurate and the number of unknowns can be greatly reduced compared with the pulse basis method to obtain the same accuracy. The simulation results show that the method is effective for forward modeling in the frequency domain and can be used to produce time domain seismograms with the Fourier transform.

INTRODUCTION

In recent years, several researchers have attempted wave equation tomography on field data with mixed results (Harris and Wang, 1993, Zhou and Schuster, 1993). Some used the time-domain waveform data to invert for velocity; others used the frequency domain wave field. In either domain, an estimate of the wave field in the inhomogenous medium is required; thus an expensive forward computation is required. To avoid this expense, approximations such as the Ray-Born algorithms for forward modeling have been developed (Beydoun and Mendes, 1987), and one way propagation methods have been proposed (Freit and Fleck, 1978, Martin and Flatte, 1988, Thomson and Chapman, 1989, Wu and Huang, 1992, Wu, 1994). However, methods that employ the ray approximation as the propagator can not treat "wave" phenomena in inhomogeneous media. In addition, the Born approximation is not valid for large scale or large contrast heterogeneities, and methods that employ the one-way propagation operator can not treat multi-reflection wave. In order to model wave propagation and scattering in arbitrarily heterogeneous media which are an important part in wave equation inversion, full wave modeling methods are required. There are two types of useful methods: One is to solve the differential form of the wave equation, e.g., with finite difference methods (Pratt, 1988), finite element methods (Robert and Andreas, 1992), or boundary element methods (Barhe, 1982). Another is to solve the integral equation (Richmond, 1965, Bojarski, 1971, Chew and Lu, 1993), in which the moment methods using pulse basis functions (Richmond, 1965) are widely used. Finite difference methods are especially useful for large areas. Conventional moment methods are especially useful for modeling in smaller regions. Also, the Frechet derivative required for inversion can be easily derived from the integral formulation.

In geophysics, our ultimate goal is inversion of the acoustic fields for earth properties; therefore, we choose the integral approach to forward modeling. It is known that the conventional pulse basis functions used in moment methods do not produce accurate representation for pixel sizes larger than about 0.1 wavelength. For large scale imaging problems, we must use many pixels and invert a huge matrix in order to find the wave field accurately in the inhomogenous medium. This is the main problem of the moment method. Up to now, many authors have attempted to improve this method (Johnson, 1983, Steinberg, 1993, Zhuck, 1994). For examples, some use wavelet expansions in the method of moments to solve a one-dimensional scattering problem (Steiberg and Leviatan, 1993), but up to now wavelet methods can only be applied when the domain of integration is a straight line or curved line (Steinberg and Leviatan, 1993, Wang, 1995). When the domain of integration is a 2_D region, no results have been reported. Undoubtedly that this type of method will be very complicated to implement in the 2-D case. By exploiting the property that any solution is composed of fast and slow spatial variations, i.e.., high and low frequency components, some anothers have applied multi-grid methods to the moment method to solve for the slow and fast modes in the solution by using iterative solvers at a coarse and fine grids, respectively (Kalbasi and Demarst, 1993). These methods greatly complicate the computation. In addition,. by the observation that the integral equation used in the method of momen (MOM) is a convolution-type integral, the K-space method which uses FFT and the conjugate gradient method has been proposed in order to accelerate the computation and reduce the memory size requirement in solving the scattering integral equation (Bojarski, 1971, 1982, 1985, Shozo and Bojarski, 1988, Borup and Gandhi, 1984, 1985, Sarkar, Ercument, Sadasiva, 1986); but for each source, almost every parameter has to be calculated again. As we know, in seismic wave inversion, there are usually 200 sources and 200 receivers, therefore, we have to repeatedly apply this method many times. This will result in great time expense. The impedance matrix in MOM does not depend on the source and receiver positions; if we use a direct matrix method such as LU decomposition, the matrix can be used to solve for fields from multiple source positions using relatively inexpensive backsubstitutions. We can also solve for the Green's functions by putting a point source at the receiver positions and using the reciprocity principle. Therefore, the moment method or the methods of solving scattering integral equation with pulse basis function is still widely used as a forward modeling method in the wave equation inversion area (Chew and Wang, 1990; Thompson, Rodi, Cheng and Toksoz, 1992; Caorsi S., Gragnani, and Pastorino, 1993; Caorsi, et al, 1994, 1995, Moghaddam and Chew, 1993, Wang and Zheng, 1992, Slvatore, Gragnani and Pastosino, 1993). As mentioned above, in applications of the MOM to the solution of the integral equations of electromagnetic or acoustic waves, ten adjustable degrees of freedom per wavelength have been the norm even for the most benign configurations (Johnson, 1983; Herrmann, 1993). The reason most commonly given for the need to oversample is that the basis functions chosen to represent scattering sources are discontinuous or have discontinuous derivatives and consequently possess a rich high-frequency spectrum (Herrmann, 1990, 1993). In this paper, we present a new variation on the moment method that is more numerically efficient for the 2-D wave propagation in strongly heterogeneous media. In our method, we discretize the integral equation on a grid and interpolate between nodes using smooth bilinear basis functions instead of pulse basis functions. In this way, we can not only increase the accuracy of the calculation of wave field, but also reduce the number of unknowns representing the field. And as pointed out above, the Frechet derivative for non-linear wave equation inversion is very easily derived.

From the numerical simulation, we observe that bilinear elements lead to a matrix with very similar properties as pulse basis matrix. Moreover it is just as easy to set up as the pulse basis function; and the linear system is just as easy to solve as that for pulse basis functions. We can get better accuracy for same amount of work using the two methods with the same pixel size, and we can use smaller impedance matrices derived by

setting the pixel size to be the wavelength divided by 6 for same accuracy as pulse method with the pixel size being the wavelength divided by 10. This great savings may enable us to use Gauss Elimination to solve linear system directly. Because the matrices derived from bilinear or pulse elements do not depend on the source and geophone position; when we apply Gauss Elimination to the matrix, we only need to do the LU factorization once, and this matrix decomposition can be used to solve for fields from multiple sources using relatively inexpensive backsubstitutions. We can also solve for the Green's functions by putting a point source at the receiver positions and using the reciprocity principle. The pulse basis method with a pixel size to obtain the same accuracy leads to a matrix which can be too large for Gauss Elimination. Therefore, the method developed here will be useful in wave field calculation in multi-source and multi-receiver system, such as cross-well imaging.

A NEW MOMENT METHOD FOR THE SCATTERING EQUATION

We restrict ourselves to the acoustic wave propagation in 2-D inhomogeneous media. In the frequency domain, we have

$$(\nabla^2 + \frac{\omega^2}{c^2(\boldsymbol{r})})u(\boldsymbol{r},\omega) = -\delta(\boldsymbol{r}-\boldsymbol{r}_s), \tag{1}$$

where, $c(\boldsymbol{r})$ is the velocity of the compression wave, $\boldsymbol{r}$ is the position vector, $\boldsymbol{r}_S$ the source position, $u(\boldsymbol{r},\omega)$ is the pressure field, and ω is the angle frequency. We define the scattering potential in terms of the contrast in velocity to be

$$M(\boldsymbol{r}) = 1 - \frac{c_o^2}{c^2(\boldsymbol{r})} \tag{2}$$

and write the total acoustic field as the sum of the incident and the scattered fields:

$$u(\boldsymbol{r}) = u^{inc}(\boldsymbol{r}) + u^{sc}(\boldsymbol{r}). \tag{3}$$

The integral equation corresponding to Eqn. (1) can be written

$$u(r) = u^{inc}(r) - k^2 \int_{\Omega} M(r')u(r',\omega)G(k|r-r'|)dr', \tag{4}$$

where $k=\omega/c_O$, Ω defines the inhomogeneous region or what we will call the object region. As shown in Figure 1, the object region is divided into R homogeneous areas, i.e., pixels, with N nodes, $\Omega = \Omega_1 \cup \Omega_2 \cdots \cup \Omega_R, \Omega_i \cap \Omega_j (i \neq j)$.

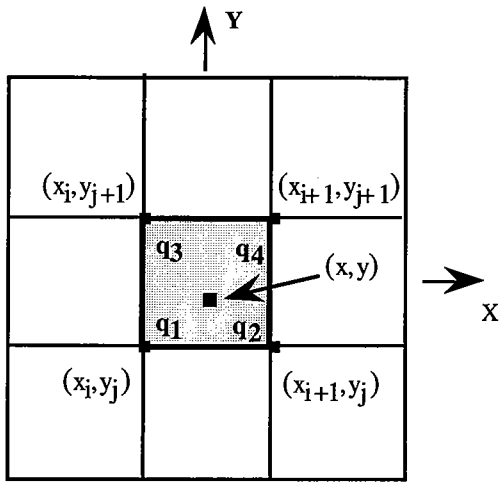

Figure 1: In the discretized form of the object region, q_1, q_2, q_3 and q_4 denote the nodes located at (x_i, y_j), (x_{i+1}, y_j), (x_i, y_{j+1}) and (x_{i+1}, y_{j+1}).

We then have

$$u(r) = u^{inc}(r) - k^2 \sum_{r=1}^{R} \int_{\Omega_r} M(r')u(r', \omega)G(k|r - r'|)dr'. \tag{5}$$

When $\boldsymbol{r'}$ is located in Ω_r, and the subscripted cartesian coordinates are used to denote the four nodes of the cell Ω_r as shown in Figure 1. We use (x, y) to denote a point within the cell and Δx and Δy the intervals in the x and y directions, respectively. When $x_i \le x \le x_{i+1}$, $y_j \le y \le y_{j+1}$, $(1 \le i \le M_x, 1 \le j \le M_y)$, define

$$\rho_l = \begin{cases} f_1 & l = (j-1) \times M_x + i \\ f_2 & l = (j-1) \times M_x + i + 1 \\ f_3 \quad \text{when} & l = (j-1) \times M_x + i + M_x \\ f_4 & l = (j-1) \times M_x + i + M_x + 1 \\ 0 & l = otherwise \end{cases} \tag{6}$$

where M_x, M_y are the total number of the nodes in the x and y direction, respectively.

$$f_1 = 1 - \frac{(x - x_i)}{\Delta x} - \frac{(y - y_j)}{\Delta y} - \frac{(x - x_i)(y - y_j)}{\Delta x \Delta y} \tag{7}$$

$$f_2 = \frac{(x - x_i)}{\Delta x} - \frac{(x - x_i)(y - y_j)}{\Delta x \Delta y} \tag{8}$$

$$f_3 = \frac{(y - y_j)}{\Delta y} - \frac{(x - x_i)(y - y_j)}{\Delta x \Delta y} \tag{9}$$

$$f_4 = \frac{(x - x_i)(y - y_j)}{\Delta x \Delta y} \tag{10}$$

The field quantities $M(\boldsymbol{r})$, $u(\boldsymbol{r})$ and $G(\boldsymbol{r};\boldsymbol{r}',k)$ are expanded using the basis function $\{\rho_n(x,y)\}$. We have

$$M(\boldsymbol{r}) = \sum_{n=1}^{N} \rho_n \cdot M_n \tag{11}$$

$$u(\boldsymbol{r},k) = \sum_{n=1}^{N} \rho_n u_n \tag{12}$$

$$G(\boldsymbol{r};\boldsymbol{r}'_j,k) = \sum_{n=1}^{N} \rho_n \cdot G_{j,n} \tag{13}$$

where N is the total number of the nodes in the object area; O_n, u_n, and $G_{j,n}$ are the values at the nodes. Substituting Eqns (11)-(13) into Eqn. (5) we obtain

$$\sum_{l=1}^{N} A_{jl} u_l + u_j = u_j^{inc} \quad (1 \le j \le N) \tag{14}$$

where N is total number of the nodes,

$$A_{jl} = \sum_{r}^{R} F_{jlr} \tag{15}$$

when $n \neq j, n \neq j-1, n \neq j-M_x-1, n \neq j-M_x$, $n = r + \text{int}eger(r/(M_x-1)),$, if $\text{mod}(r, M_x-1) \neq 0$, $n = r + \text{int}eger(r/(M_x-1)) - 1$, if $\text{mod}(r, M_x-1) = 0$, we have (see Appendix **1**)

$$F_{jlr} = B_{j,n}\delta_{l,n} + C_{j,n+1}\delta_{l,n+1} + D_{j,n+Mx}\delta_{l,n+Mx} + E_{j,n+Mx+1}\delta_{l,n+Mx+1} \tag{16}$$

$$\delta_{i,j} = \begin{cases} 1 & i = j \\ 0 & \text{i} \neq \text{j} \end{cases} \tag{17}$$

where

$$\begin{aligned} B_{j,n} = \{&\tfrac{1}{16}Q_1(q_1)Q_2(q_1) + \tfrac{1}{48}[Q_1(q_2)Q_2(q_2) + Q_1(q_3)Q_2(q_3) + Q_1(q_2)Q_2(q_1) + \\ &Q_1(q_1)Q_2(q_2) + Q_1(q_3)Q_2(q_1) + Q_1(q_1)Q_2(q_3)] + \tfrac{1}{144}[Q_1(q_4)Q_2(q_4) + \\ &Q_1(q_4)Q_2(q_1) + Q_1(q_4)Q_2(q_3) + Q_1(q_1)Q_2(q_4) + Q_1(q_2)Q_2(q_3) + \\ &Q_1(q_2)Q_2(q_4) + Q_1(q_3)Q_2(q_2) + Q_1(q_3)Q_2(q_4) + Q_1(q_4)Q_2(q_2)]\}\Delta x\Delta y k^2 \end{aligned} \tag{18}$$

$$\begin{aligned} C_{j.n+1} = \{&\tfrac{1}{16}Q_1(q_2)Q_2(q_2) + \tfrac{1}{48}[Q_1(q_1)Q_2(q_1) + Q_1(q_4)Q_2(q_4) + Q_1(q_2)Q_2(q_1) + \\ &Q_1(q_1)Q_2(q_2) + Q_1(q_4)Q_2(q_2) + Q_1(q_2)Q_2(q_4)] + \tfrac{1}{144}[Q_1(q_3)Q_2(q_3) + \\ &Q_1(q_3)Q_2(q_1) + Q_1(q_1)Q_2(q_3) + Q_1(q_4)Q_2(q_1) + Q_1(q_1)Q_2(q_4) + \\ &Q_1(q_2)Q_2(q_3) + Q_1(q_3)Q_2(q_2) + Q_1(q_4)Q_2(q_3) + Q_1(q_3)Q_2(q_4)]\}\Delta x\Delta y \end{aligned} \tag{19}$$

$$D_{j,n+M_x} = \{\tfrac{1}{16}Q_1(q_3)Q_2(q_3)+\tfrac{1}{48}[Q_1(q_1)Q_2(q_1)+Q_1(q_4)Q_2(q_4)+Q_1(q_4)Q_2(q_3)+ Q_1(q_3)Q_2(q_4)+Q_1(q_3)Q_2(q_1)+Q_1(q_1)Q_2(q_3)]+\tfrac{1}{144}[Q_1(q_2)Q_2(q_2)+ Q_1(q_2)Q_2(q_1)+Q_1(q_1)Q_2(q_4)+Q_1(q_2)Q_2(q_3)+Q_1(q_1)Q_2(q_2)+ Q_1(q_4)Q_2(q_1)+Q_1(q_3)Q_2(q_2)+Q_1(q_4)Q_2(q_2)+Q_1(q_2)Q_2(q_4)]\}\Delta x\Delta y k^2 \quad (20)$$

and

$$E_{j,n+M_x+1} = \{\tfrac{1}{16}Q_1(q_4)Q_2(q_4)+\tfrac{1}{48}[Q_1(q_2)Q_2(q_2)+Q_1(q_3)Q_2(q_3)+Q_1(q_2)Q_2(q_4)+ Q_1(q_4)Q_2(q_3)+Q_1(q_4)Q_2(q_2)+Q_1(q_3)Q_2(q_4)]+\tfrac{1}{144}[Q_1(q_2)Q_2(q_1)+ Q_1(q_1)Q_2(q_4)+Q_1(q_1)Q_2(q_2)+Q_1(q_1)Q_2(q_3)+Q_1(q_4)Q_2(q_1)+ Q_1(q_3)Q_2(q_1)+Q_1(q_3)Q_2(q_2)+Q_1(q_1)Q_2(q_1)+Q_1(q_2)Q_2(q_3)]\}\Delta x\Delta y k^2 \quad (21)$$

where $Q_1(q_i) = G_{j,q_i}$ and $Q_2(q_i) = M_{q_i}$.,and $R = (M_x - 1)\times(M_y - 1)$,, and the definitions of q_i are shown in Figure 1. When $n = j, n = j-1, n = j-M_x-1, n = j-M_x$, the Green functions have a singularity, but using the same method as in the paper (Richmond, 1965) for singularity processing, we have

$$F_{jlr} = \frac{i}{2}[\pi k a H_0^{(1)}(ka)+2i] * M_l\delta_{l,n} \quad (22)$$

where $a = \sqrt{\Delta x\cdot\Delta y/\pi}$. Thus, equation (14) can be written as

$$\Gamma \boldsymbol{U} = \boldsymbol{U}^{inc} \quad (23)$$

where $\boldsymbol{U} = (u_1, u_2, \cdots, u_N)^t, \boldsymbol{U}^{inc} = (u_1^{inc}, u_2^{inc}, \cdots, u_N^{inc})^t, \Gamma_{jl} = A_{jl}$, $(j \neq l)$, $\Gamma_{jl} = A_{jl} + 1.$, $(j = l)$ Therefore, the total field can be obtained by solving equation (23) and we solve the linear system (23) for $\boldsymbol{U}$ using Gaussian Elimination; we will discuss the numerical solution of (23) in the next section.

After the total field is found, the scattering field at r_m outside the object region can be expressed as

$$u_m^{sc} = -\sum_{l=1}^{N} A_{ml}M_l \quad (24)$$

where A_{ml} equals Eqn (14), and $Q_1(q_i) = G_{m,q_i}$, $Q_2(q_i) = u_{q_i}$. Therefore, the scattering field in frequency domain can be derived by Eqn (24) and the waveform of the scattering can be derived by inverse Fourier transform of the frequency domain wave field.

NUMERICAL SIMULATIONS

We used our bilinear method to calculate the scattered fields for the two models shown in Figures 2a and 3a. The velocities, along with the geometry of the source and receiver positions, are denoted in the figures. 100 sources and 100 receivers are located at x=-30 m and x=+30m at equal z-axis intervals of 1.6 m. This geometry corresponds to the

crosswell imaging experiment in borehole geophysics. We compare pulse basis simulations with the bilinear basis simulations. First, we discuss the properties of the matrices derived by the two different basis functions. When we use the same size model with (Mx+1)*(My+1) nodes, then we can establish two impedance matrices for the pulse element method and bilinear element method, which we call Γ_0, $n_0 \times n_0$,, where $n_0 = Mx \times My$ for the pulse element method, and Γ, $n \times n$, where $n = (Mx+1) \times (My+1)$ for the bilinear element method. When we set the unknown number of elements in two different formulations to make $n_0 = n$, then, Γ_0 and Γ are very similar: (1) For model II, both of matrices we obtained from pulse elements and bilinear elements are very well conditioned; the condition numbers of bilinear element matrix and pulse element matrix are 4.3 and 5.8, respectively; and the matrix Γ for bilinear element is slightly better conditioned than Γ_0; and $\|\Gamma - \Gamma_0\|_2 / \|\Gamma_0\|_2 = 0.085$, which shows that the matrices are not dissimilar; and (2) the distribution of the singular values corresponding to both the largest and smallest singular values are also almost identical. Therefore, solving linear systems of the same size with Γ and Γ_0 will be of equivalent difficulty whether we use Gauss Elimination with pivoting or an iterative method like generalized minimum residual method (GMRES) (Youcef and Schultz, 1986, Walker, 1989, Navarra, 1989), which is appropriate for non-singular matrices with no special properties such as symmetry or positive definitions. Since the matrix is dense, we don't expect iterative method will be better than Gauss elimination when you can use Gauss Elimination. We find that to obtained the desired accuracy, for example, in a cross well imaging system, the matrix for bilinear is not too big to use Gauss Elimination.

In addition, one main advantage of Gauss Elimination is that once we do the LU factorization, we can solve many linear systems with same matrix and many different right hand sides, while an iterative solver will be expensive for multi-source/multi-receiver systems because for different source or receiver, the wave field must be solve independedly. Any method we can use for Γ_0 , we can also use for Γ. For the same size of cell, the moment method with bilinear basis functions get better accuracy than that with pulse basis functions To get same accuracy, the moment method with bilinear basis functions requires a smaller matrix than for the pulse basis functions, as the following numerical experiments shown

With pulse basis functions, we use 10 pixels per wavelength, while with the bilinear basis function we use only 6 nodes per wavelength. A comparison of the results is shown in Figures 2b-2f and 3b-3f.

Model I (Figure 2) consists of a rectangular block centered at x=1.6m , z=0.0 m in an otherwise homogeneous medium. We plot in Figure 2b the magnitude of the amplitude at all receivers for the source at z=0. m. If we assume that the more expensive pulse basis simulation is accurate (Johnson, 1983, Herrmann, 1993), then we find that the bilinear basis functions yield errors less than approximately 5.3 % everywhere (Figure 2b). However, the bilinear basis simulation requires less memory to store the matrix for inversion than pulse basis simulation. Therefore, it can run greatly faster than the pulse basis simulation when solving the linear system (23) for the total field in the medium. Compared with pulse basis simulation, the larger the inhomogeneous region is, the faster the bilinear simulation is. Here, the bilinear simulation is about 60% faster than the pulse basis simulation. The real and imaginary parts of the computed scattered amplitudes for the 100x100 source-receiver positions are displayed in Figures 2c and 2d for the bilinear basis functions, and in Figures 2e and 2f for the pulse basis functions. The patterns of amplitudes are obviously very similar in both simulations.

Model II is more geological in origin (Figure 3a). A line plot of the amplitude for the source at z=80m is shown in Figure 3b, where again we have error of less than about 4.8 %. The real and imaginary amplitudes of the scattered wave field are displayed in Figures 3c and 3d for the bilinear basis functions and Figures 3e and 3f for the pulse basis functions. Again, as with Model I, there is excellent similarity between the two. For inversion, we often need to know the fields everywhere in the region. In Figures 4a to 4d, we display the total field magnitude at every pixel or node on the solution grid for a source at z=80m by using the bilinear basis function moment method and the pulse moment method. This comparison illustrates the uniformity of the results for regions both near and far away form the source.

Finally, we applied the inverse Fourier transform to the frequency domain scattered wave field of both Models I and II to obtain the time domain waveforms or seismograms. These are shown in Figures 5a and 5b for the one common shot gather for Model I and II, respectively. We used a Ricker wavelet (first derivative of a Gaussian) with a 300 Hz center frequency and nodes of $\Delta x = \Delta y = 1/6 \times \lambda_{min}$. The seismogram for Model I shows the typical hyperbolic moveout of a diffraction from a small object embedded in a homogeneous medium. The seismogram for the layered model is more complicated, exhibiting clear reflections and diffractions.

CONCLUSIONS

We described a new moment method for evaluating the wave field in inhomogeneous media. We used a bilinear basis function to discretize the acoustic integral equation and compute the area integration for each small square cell instead of approximating the pixels with circular cells everywhere as with pulse basis functions, except in the singularities. With this method, the wave field can be calculated accurately for only 6 nodes per wavelength instead of 10 pixels per wavelength with the pulse basis function. As a result, the memory requirements and execution times for numerical implementation is significantly deceased, while the errors are usually less than 6%. If there are less than 6 nodes per wavelength in the bilinear simulation, the storage and execution time can be further reduced, but the simulation precision will be decreased also. In addition, the Frechét derivative for non-linear wave equation inversion is easy to derive from our bilinear basis simulation. Numerical simulations show our method is effective and very useful in solving forward scattering problem. Although bilnear basis element have been used previously in many other application, we have demonstrated here that their application to the method of moments, where the current standard method uses pulse basis functions, leads to discrete problems which are just as easy to set up and solve as with pulse basis functions; moreover the solution with bilinear elements are much more accurate for the same level of discretization, and thus are less expensive because we can use larger pixel sizes to obtain accuracy equivalent to the standard pulse basis function method.

ACKNOWLEDGMENTS

This work was supported by the Seismic Tomography Project of Stanford University, a research consortium sponsored by companies of the oil and gas industry.

REFERENCES

Bathe, K.J., Finite Element Procedures in Engineering Analysis, Englewood Cliffs, NJ: Prentice Hall, Inc., 1982

Beydoun, W.B. and M. Mendes, Elastic ray Born l^2 migration / inversion, Geophys, J., 97, 151-160

Bojarski, N.N., K-space formulation of the electromegnetic scattering problem, Rep. AFAL-TR-71-75, AIR Force Avionics Lab., Wright-patterson Air Force Base, Ohio, March, 19971

Bojarski, N.N., The k-space formulation of the scattering problem in the time domain: An improved single propagator formulation, J. Acous. Soc. Am. 77(3), 826-831, 1985

Bojarski, N.N., The k-space formulation of the scattering problem in the time domain, J Acous Soc. AM, 72(2), 570-584, 1982

Borup, D.T., and O.P. Gandhi, Fast-Fourier-transform method for calculation of SAR distribution in finely discretized inhomogeneous models of biological bodies, IEEE Trans. Microwave Theory Tech., MIT-32, 355-360, 1984

Borup, D.T., and O.P. Gandhi, Calculation of high-resultion SAR distribution in biological bodies using the FFT algorithm and the conjugation gradient method,, IEEE Trans. Microwave Theory Tech., MIT-33, 417-419, 1985

Caorsi S., Gragnani G.L., and Pastorino M., Redundant Electromagnetic data for microwave imaging of three-dimensional dielectric objects, IEEE Transactions on Atennas and Propgation, Vol.42, No.5, 581-589, 1993.

Caorsi S. , Gragnani, G.L., Pastorino M. and Zunino G., Microwave Imaging Based on a Markov Random Field model, IEEE Transaction on Atennas and propagation, Vol. 42, No.3, 29-303, 1994

Caorsi S., Gragnani G.L., Medicina, S., Pastorino M., and Pinto, G.A., A Gibbs random fielfd-based active electromegnetic method for noninvasive diagnostics in biomedical applications, Radio Science, Vol.30, No. 1, 291-301, 1995

Chew W. C. and Cai-cheng Lu, The use of Huygens' Equivalence principle for solving the volume integral equation of scattering, IEEE Transaction on antennas and propagation, vol. 41, no.7, 897-904,1993

Chew W.C. and Y.M. Wang, Reconstruction of Two-Dimensional permittivity distribution using the Distorted Born iterative method, IEEE transactions on medical imaging, Vol. 9, No.2, 218-235, 1990

Denis F. and Basset O. and Gimenez G., Ultrasonic Transmission tomography in Refracting media: Reduction of Refraction artifacts by curved-ray techniques, IEEE Transactions on Atennas and Propgation, Vol.41, No. 1, 1993.

Feit, M. D., and Fleck, J.A. Jr., Light propagation in graded-index optical fibers: Applied Opticcs, 17, 3990-3998, 1978.

Harris, J. M and Guang Wang, Diffraction tomography for inhomogeneities in a layered background, Expanded Abstract of 63rd Annual meeting of Soiety of Exploration Geophysics, 49-52, 1993

Herrmann, G.F. and Strain S.M., Sampling method using prefiltered Band-limited Green's functions for the solution of electromagnetic integral equations, IEEE Transactions on Atennas and Propgation, Vol.41, No. 1, 20-24, 1993.

Herrmann, G.F., Note on Interpolational Basis functions in the Mothod of Moments, IEEE Transactions on Atennas and Propgation, Vol.38, No. 1, 134-137,1990.

Johnson, Steven A. and Michael L. Tracy, Inverse Scattering solution by a sinc basis, multiple source, moment method --Part I : Theory, Ultrosonic Imaging 5, 361-375, 1983

Khahil Kalbasi, and Kenneth R. Demarst, A multilevel formulation of the method of moments, IEEE Transactions on Atennas and Propgation, Vol.41, No. 5, 589-599, 1993.

LEE Robert, and Cangellaris Andreas C., A study of discretization Error in the finit element approximation of wave solutions. IEEE Transactions on Atennas and Propgation, Vol.40, No.5, 542-555, 1992.

Moghaddam, Maha , and Weng Cho Chew, Study of some practical issues in inversion with the Born Iterative method using Time-Domain Data, IEEE Transactions on Atennas and Propgation, Vol.41, No. 2, 177-184, 1993.

Martin, J.M., and Flatte, S.M., Intensity images and statistics from numerical simulation of wave propagation in 3-D radom media: Applied Optics, 27, 2111-2126, 1988

Navarra Antonio, An application of GMRES to indefinite linear problems in meteorolgy, Computer Physics Communicatios, 53, 321-327, 1989,

Zhuck, Nickolay P and Alexander G. Yarovoy, Two-dimensional scattering from an inhomogeneous dielectric cylinder embedded in a stratified medium: Case of TM polarization, IEEE Transaction on antennas and propagation, vol. 42, no.1, 1994.

Pratt, R.G., Frequency-domain elastic wave modeling by finite differences: A tool for crosshole seismic imaging, Geophysics 55: 626-623, 1990

Richmond, J.H., Scattering by a dielectric cylinder of arbitary cross section shape, IEEE Trans, Ant. Prop. 13:334-341, 1965

Sarkar Tapan K, Arvas Ercument , and Rao Sadasiva M., Application of FFT and the conjugation grdient method for the solution of electromagnetic radiation from electrically large and small conducting bodies, IEEE transactions on atennas and propagation, Vol. AP-34, No.33, 635-640,1986

Shozo Koshigoe, Bojarski, N.N., The k-space formulation of the acoustic scattering problem, J. Acoust. Sco. Am. 84(5), 1890-1893, 1988

Slvatore Caorsi, Gian Luigi Gragnani, and Matteo Pastorino, Reconstruction of Fielectric permittivity distributions in arbitrary 2-D inhomogeneous biological bodies by a multiview microwave numerical method, IEEE transactions on medical imaging, Vol. 12, No.2, 1993

Steiberg B.Z. and Leviatan Yehuda , On the use of Wavelet expansions in the method of moments, IEEE Transaction on antennas and propagation, vol. 41, no.5, 1993

Thompson, R.D, W.L.Rodi, C.H. Cheng anf M.N. Toksoz, Nonlinear Diffraction Tomography Applied to Crosshole Seismic Data, Geotomography, Vol. 2, 445-456,1992(The Proceedings of The Second SEGJ/SEG International Symposium on Geotomography)

Thomson, D.J., and Chapman, N.R., , A wide angle algorithm for the parabolic equation: J. Acoust. Soc. Am. 74, 1848-1854, 1983.

Walker F. Homer, Implementations of the GMRES method, Computer Physics Communications 53, 311-320, 1989

Wang Gaofeng, Hybrid wavelet expansion and boundary element analyssis of electromagnetic scattering from conducting objects, IEEE Transactions on Atennas and Propagation, Vol. 43, No.2, 170-178, 1995.

Wang Weiyan and Zhang Shourong, Unrelated Illumination Method for electromagnteic inverse scattering of inhomogeneous lossy dielectric bodies, IEEE Transactions on Atennas and Propgation, Vol.40, No.11, 1292-1296, 1992.

Wu, R.S., 1994, Wide-angle elastic wave one-way propagation in heterogeneous media and an elastic wave complex-screen method, J. Geophys. Res., 99, 751-766, 1994

Wu, R.S. and Huang, L.J., 1992, Scattered field calculation in heterogeneous media using phase-screen propagator, Expanded Abstracts of the technical program, SEG 62th Annual Meeting, 1289-1292.

Youcef saad and Martin H. Schultz, GMRES: A generalized minimal residual algorithm for solving nonsymmetric linear systems, SIAM J. SCI. STAT. COMPUT., Vo. 7, No. 3, 1986

Zhou Changxi and Gerard T. schuster, Waveform Inversion of Subwell velocity, Exapanded Abstract of 63rd Annual Meeting of Society of Exploration of Geophysics, 106-109, 1993.

Appendix 1

When inserting equations (11) - (13) into the integration in equation (5), we have

$$\int_{x_i}^{x_i+\Delta x}\int_{y_i}^{y_i+\Delta y} M(\boldsymbol{r}')G(k|\boldsymbol{r}-\boldsymbol{r}'|)U(\boldsymbol{r}',\omega)d\boldsymbol{r}' = \int_{x_i}^{x_i+\Delta x}\int_{y_i}^{y_i+\Delta y} (\sum_{n=1}^{N}\rho_n M_n)\cdot(\sum_{n=1}^{N}\rho_n u_n)\cdot(\sum_{n=1}^{N}\rho_n G_n)dx'dy'$$

$$= \int_{x_i}^{x_i+\Delta x}\int_{y_i}^{y_i+\Delta y} (\rho_n M_n + \rho_{n+1}M_{n+1} + \rho_{n+M_x}M_{n+M_x} + \rho_{n+M_x+1}M_{n+M_x+1})\cdot$$

$$(\rho_n G_n + \rho_{n+1}G_{n+1} + \rho_{n+M_x}G_{n+M_x} + \rho_{n+M_x+1}G_{n+M_x+1})\cdot$$

$$(\rho_n u_n + \rho_{n+1}u_{n+1} + \rho_{n+M_x}u_{n+M_x} + \rho_{n+M_x+1}u_{n+M_x+1})\,dx'dy'$$

where $n=(j-1)\cdot M_x + i$ Define
$Q_1 = G, Q_2 = M, l = q_1, l+1 = q_2, l+M_x = q_3, l+M_x+1 = q_4$, we have

$$\int_{x_i}^{x_i+\Delta x}\int_{y_i}^{y_i+\Delta y} M(\boldsymbol{r}')G(k|\boldsymbol{r}-\boldsymbol{r}'|)U(\boldsymbol{r}',\omega)d\boldsymbol{r}' =$$

$$\int_{x_i}^{x_i+\Delta x}\int_{y_i}^{y_i+\Delta y} [(\rho(q_1)\rho(q_1)Q_1(q_1)Q_2(q_1) + \rho(q_2)\rho(q_1)Q_1(q_2)Q_2(q_1) + \rho(q_3)\rho(q_1)Q_1(q_3)Q_2(q_1)$$

$$(\rho(q_1)Q_2(q_1) + \rho(q_2)Q_2(q_2) + \rho(q_3)Q_2(q_3) + \rho(q_4)Q_2(q_4))\cdot]$$

$$(\rho(q_1)u(q_1) + \rho(q_2)u(q_2) + \rho(q_3)u(q_3) + \rho(q_4)u(q_4))\,dx'dy'$$

$$= \int_{x_i}^{x_i+\Delta x}\int_{y_i}^{y_i+\Delta y} [(\rho(q_1)\rho(q_1)Q_1(q_1)Q_2(q_1) + \rho(q_2)\rho(q_1)Q_1(q_2)Q_2(q_1) + \rho(q_3)\rho(q_1)Q_1(q_3)Q_2(q_1)$$

$$+\rho(q_4)\rho(q_1)Q_1(q_4)Q_2(q_1))\cdot(\rho(q_1)\rho(q_2)Q_1(q_1)Q_2(q_2) + \rho(q_2)\rho(q_2)Q_1(q_2)Q_2(q_2)$$

$$+\rho(q_3)\rho(q_2)Q_1(q_3)Q_2(q_2) + \rho(q_4)\rho(q_2)Q_1(q_4)Q_2(q_2))\cdot(\rho(q_1)\rho(q_3)Q_1(q_1)Q_2(q_3)$$

$$+\rho(q_2)\rho(q_3)Q_1(q_2)Q_2(q_3) + \rho(q_3)\rho(q_3)Q_1(q_3)Q_2(q_3) + \rho(q_4)\rho(q_3)Q_1(q_4)Q_2(q_3))\cdot$$

$$(\rho(q_1)\rho(q_4)Q_1(q_1)Q_2(q_4) + \rho(q_2)\rho(q_4)Q_1(q_2)Q_2(q_4) + \rho(q_3)\rho(q_4)Q_1(q_3)Q_2(q_4)$$

$$+\rho(q_4)\rho(q_4)Q_1(q_4)Q_2(q_4))]\cdot(\rho(q_1)u(q_1) + \rho(q_2)u(q_2) + \rho(q_3)u(q_3) + \rho(q_4)u(q_4))\cdot dx'dy'$$

$$= \int_{x_i}^{x_i+\Delta x} \int_{y_i}^{y_i+\Delta y} \{[(\rho(q_1)\rho(q_1)\rho(q_1)Q_1(q_1)Q_2(q_1) + \rho(q_2)\rho(q_1)\rho(q_1)Q_1(q_2)Q_2(q_1)$$

$$+\rho(q_3)\rho(q_1)\rho(q_1)Q_1(q_3)Q_2(q_1) + \rho(q_4)\rho(q_1)\rho(q_1)Q_1(q_4)Q_2(q_1)) \cdot$$

$$+\rho(q_3)\rho(q_2)\rho(q_1)Q_1(q_3)Q_2(q_2) + \rho(q_4)\rho(q_2)\rho(q_1)Q_1(q_4)Q_2(q_2)) \cdot$$

$$(\rho(q_1)\rho(q_4)\rho(q_1)Q_1(q_1)Q_2(q_4) + \rho(q_2)\rho(q_4)\rho(q_1)Q_1(q_2)Q_2(q_4)$$

$$+\rho(q_3)\rho(q_4)\rho(q_1)Q_1(q_3)Q_2(q_4) + \rho(q_4)\rho(q_4)\rho(q_1)Q_1(q_4)Q_2(q_4))] \cdot u(q_1)$$

$$+[(\rho(q_1)\rho(q_1)\rho(q_2)Q_1(q_1)Q_2(q_1) + \rho(q_2)\rho(q_1)\rho(q_2)Q_1(q_2)Q_2(q_1)$$

$$+\rho(q_3)\rho(q_1)\rho(q_2)Q_1(q_3)Q_2(q_1) + \rho(q_4)\rho(q_1)\rho(q_2)Q_1(q_4)Q_2(q_1)) \cdot$$

$$(\rho(q_1)\rho(q_2)\rho(q_2)Q_1(q_1)Q_2(q_2) + \rho(q_2)\rho(q_2)\rho(q_2)Q_1(q_2)Q_2(q_2)$$

$$+\rho(q_3)\rho(q_2)\rho(q_2)Q_1(q_3)Q_2(q_2) + \rho(q_4)\rho(q_2)\rho(q_2)Q_1(q_4)Q_2(q_2)) \cdot$$

$$(\rho(q_1)\rho(q_3)\rho(q_2)Q_1(q_1)Q_2(q_3) + \rho(q_2)\rho(q_3)\rho(q_2)Q_1(q_2)Q_2(q_3)$$

$$(\rho(q_1)\rho(q_4)\rho(q_2)Q_1(q_1)Q_2(q_4) + \rho(q_2)\rho(q_4)\rho(q_2)Q_1(q_2)Q_2(q_4)$$

$$+\rho(q_3)\rho(q_4)\rho(q_2)Q_1(q_3)Q_2(q_4) + \rho(q_4)\rho(q_4)\rho(q_2)Q_1(q_4)Q_2(q_4))] \cdot u(q_2)$$

$$[(\rho(q_1)\rho(q_1)\rho(q_3)Q_1(q_1)Q_2(q_1) + \rho(q_2)\rho(q_1)\rho(q_3)Q_1(q_2)Q_2(q_1)$$

$$+\rho(q_3)\rho(q_1)\rho(q_3)Q_1(q_3)Q_2(q_1) + \rho(q_4)\rho(q_1)\rho(q_3)Q_1(q_4)Q_2(q_1)) \cdot$$

$$(\rho(q_1)\rho(q_2)\rho(q_3)Q_1(q_1)Q_2(q_2) + \rho(q_2)\rho(q_2)\rho(q_3)Q_1(q_2)Q_2(q_2)$$

$$+\rho(q_3)\rho(q_2)\rho(q_3)Q_1(q_3)Q_2(q_2) + \rho(q_4)\rho(q_2)\rho(q_3)Q_1(q_4)Q_2(q_2)) \cdot$$

$$(\rho(q_1)\rho(q_3)\rho(q_3)Q_1(q_1)Q_2(q_3) + \rho(q_2)\rho(q_3)\rho(q_3)Q_1(q_2)Q_2(q_3)$$

$$+\rho(q_3)\rho(q_3)\rho(q_3)Q_1(q_3)Q_2(q_3) + \rho(q_4)\rho(q_3)\rho(q_3)Q_1(q_4)Q_2(q_3)) \cdot$$

$$(\rho(q_1)\rho(q_4)\rho(q_3)Q_1(q_1)Q_2(q_4) + \rho(q_2)\rho(q_4)\rho(q_3)Q_1(q_2)Q_2(q_4)$$

$$+\rho(q_3)\rho(q_4)\rho(q_3)Q_1(q_3)Q_2(q_4) + \rho(q_4)\rho(q_4)\rho(q_3)Q_1(q_4)Q_2(q_4))] \cdot u(q_3)$$

$$+[(\rho(q_1)\rho(q_1)\rho(q_4)Q_1(q_1)Q_2(q_1) + \rho(q_2)\rho(q_1)\rho(q_4)Q_1(q_2)Q_2(q_1)$$

$$+\rho(q_3)\rho(q_1)\rho(q_4)Q_1(q_3)Q_2(q_1) + \rho(q_4)\rho(q_1)\rho(q_4)Q_1(q_4)Q_2(q_1)) \cdot$$

$$(\rho(q_1)\rho(q_2)\rho(q_4)Q_1(q_1)Q_2(q_2)+\rho(q_2)\rho(q_2)\rho(q_4)Q_1(q_2)Q_2(q_2)$$

$$+\rho(q_3)\rho(q_2)\rho(q_4)Q_1(q_3)Q_2(q_2)+\rho(q_4)\rho(q_2)\rho(q_4)Q_1(q_4)Q_2(q_2))\cdot$$

$$(\rho(q_1)\rho(q_3)\rho(q_4)Q_1(q_1)Q_2(q_3)+\rho(q_2)\rho(q_3)\rho(q_4)Q_1(q_2)Q_2(q_3)$$

$$+\rho(q_3)\rho(q_3)\rho(q_4)Q_1(q_3)Q_2(q_3)+\rho(q_4)\rho(q_3)\rho(q_4)Q_1(q_4)Q_2(q_3))\cdot$$

$$(\rho(q_1)\rho(q_4)\rho(q_4)Q_1(q_1)Q_2(q_4)+\rho(q_2)\rho(q_4)\rho(q_4)Q_1(q_2)Q_2(q_4)$$

$$+\rho(q_3)\rho(q_4)\rho(q_4)Q_1(q_3)Q_2(q_4)+\rho(q_4)\rho(q_4)\rho(q_4)Q_1(q_4)Q_2(q_4))]\cdot u(q_4)\ \}\cdot dx'dy'$$

$$=B_{q_1}u(q_1)+C_{q_2}u(q_2)+D_{q_3}u(q_3)+E_{q_4}u(q_4)$$

the defnitions of $B_{q_1}, C_{q_2}, D_{q_3}, E_{q_4}$ are shown by equations (18)-(21)

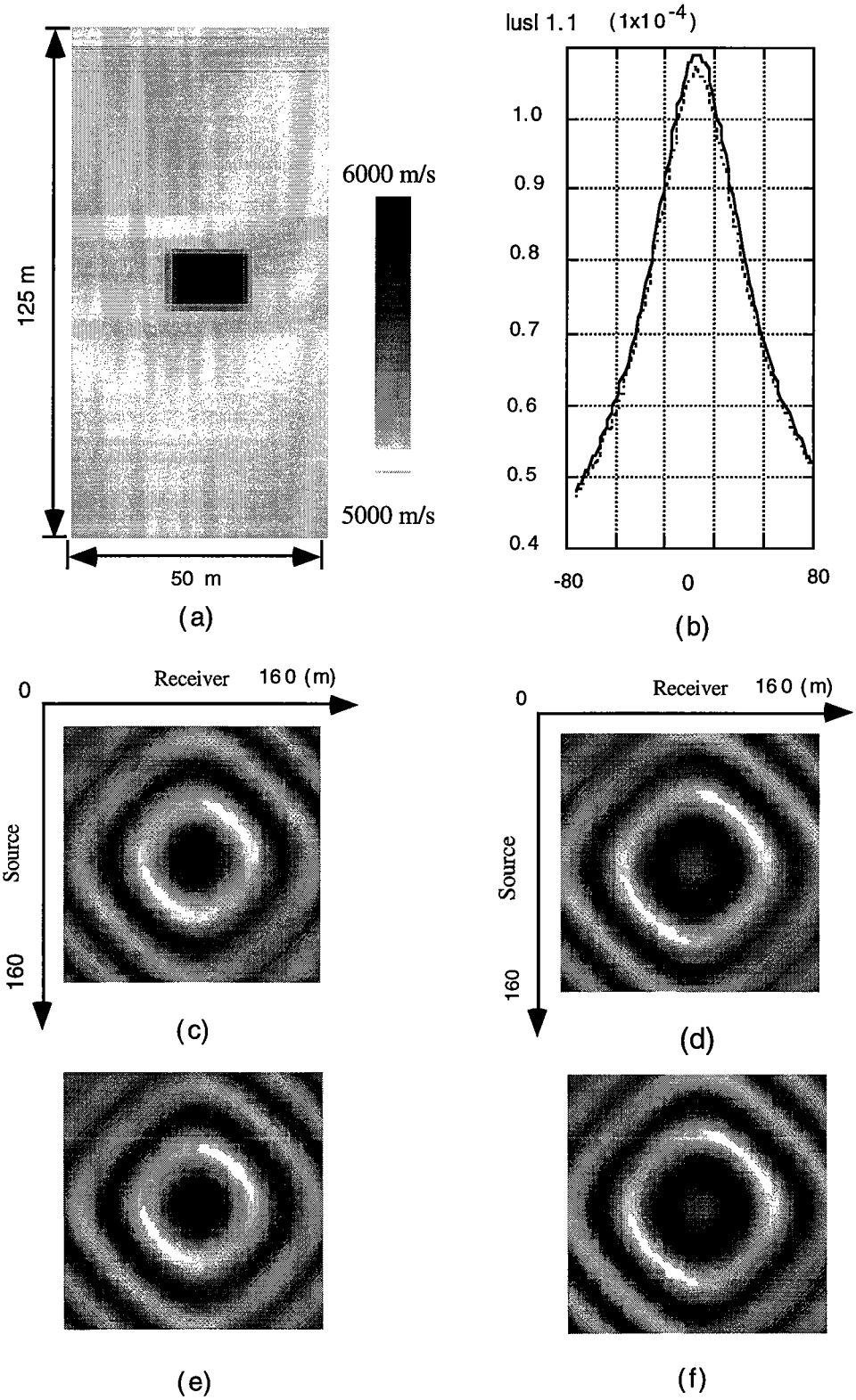

Figure 2: (a) Synthetic model I. (b) The amplitudes of the received sacattered fields for the bilinear and pulse basis functions moment methods, where dot and dense lines denote the results of the blinear and pulse basis function moments methods, respectively, and the source is located at (0,0); (c) and (d) display the real and imaginary parts of the computed scattered amplitudes for the 100 x100 source-receiver positions for the binear basis functions, the results in (e) and (f) are for the pulse basis functions.

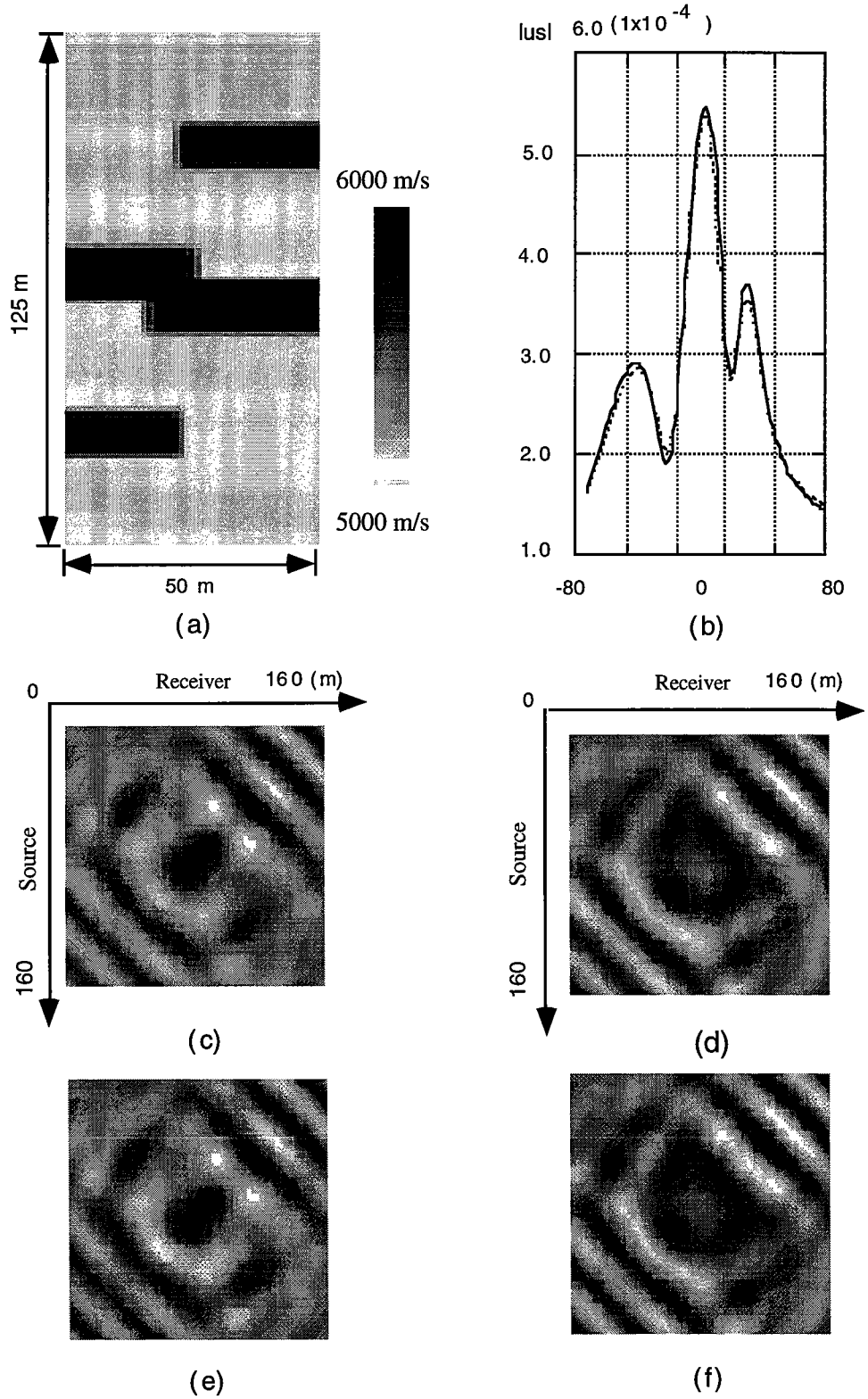

Figure 3: (a) Synthetic model II. (b) The amplitudes of the received sacattered fields for the bilinear and pulse basis functions moment methods, where dot and dense lines denote the results of the blinear and pulse basis function moments methods, respectively, and the source is located at (0,0); (c) and (d) display the real and imaginary parts of the computed scattered amplitudes for the 100 x100 source-receiver positions for the binear basis functions, the results in (e) and (f) are for the pulse basis functions.

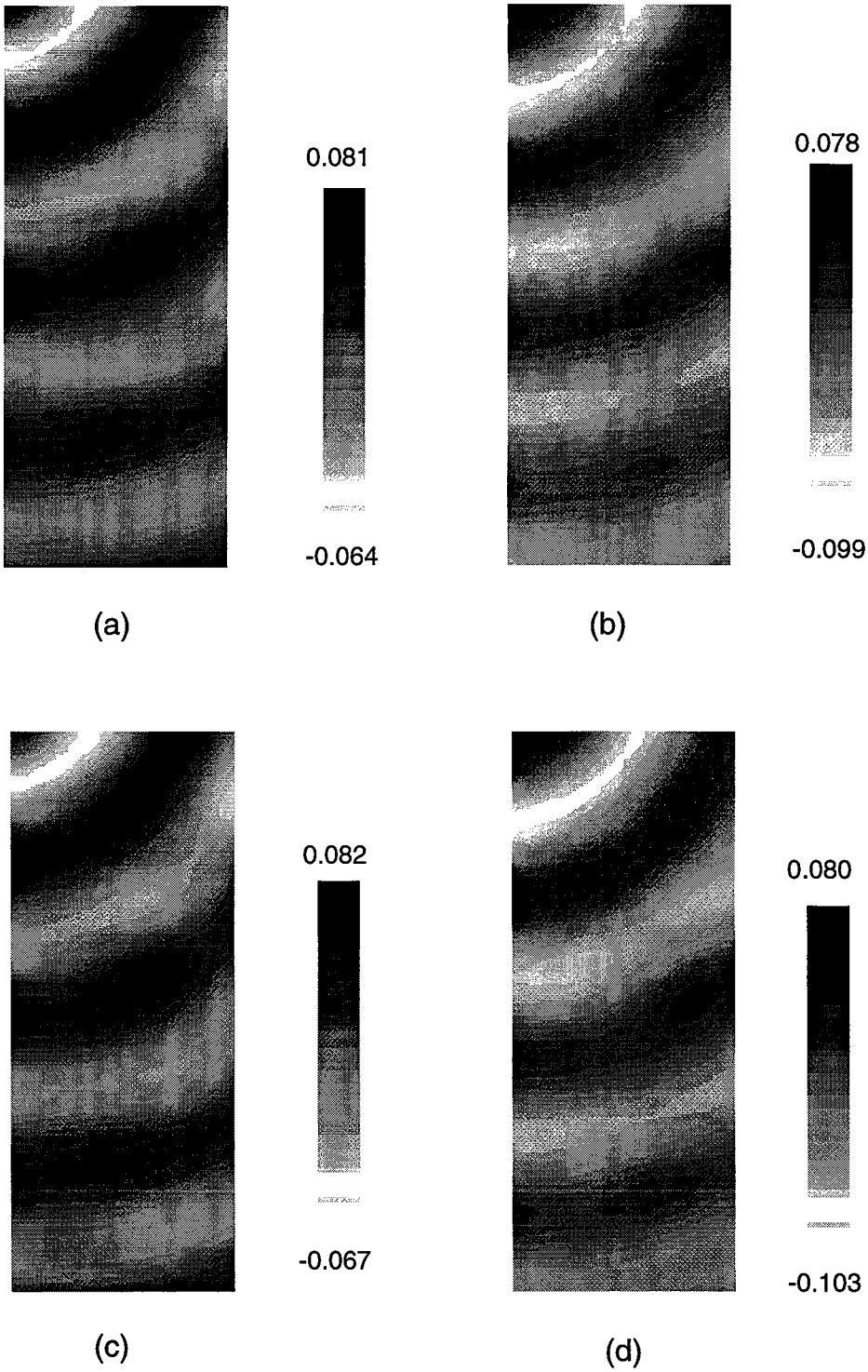

Figure 4: (a) and (b) are the real and imaginary part of the total field of model II in the object region derived by the bibinear basis function moment method, respectively; (c) and (d) are the real and imaginary part of the total field of model II in the object region derived by the pulse basis function moment method, respectively, and in the (a) -(d), theposition of the source is (-30,80).

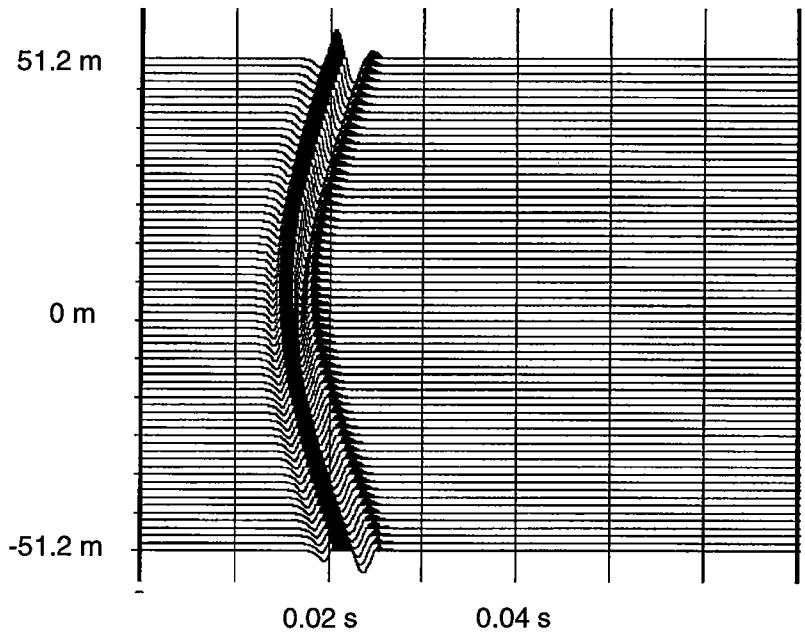

(a)

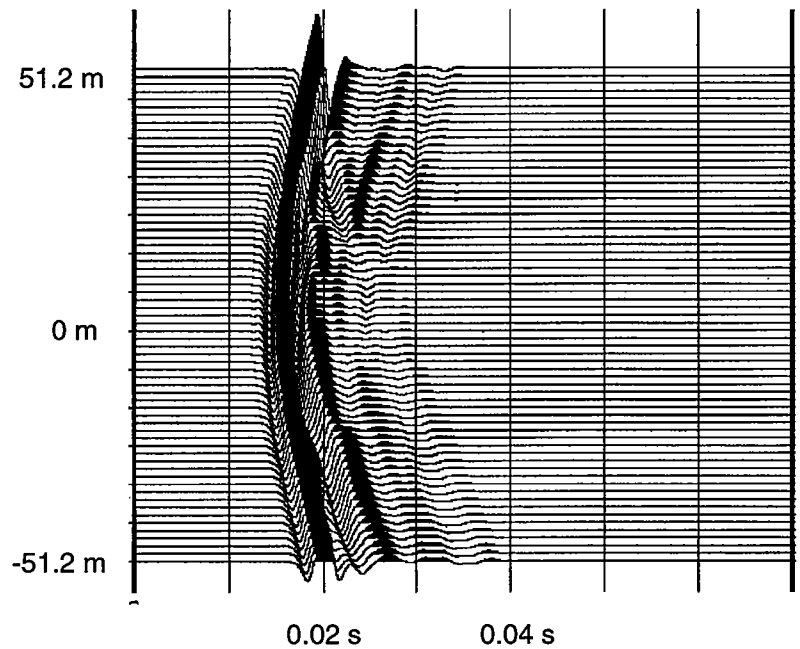

(b)

Figure 5: (a) The waveform of the scattered field by model I. (b) The waveform of the scattered field by model II